Teagle, D.A.H., Wilson, D.S., Acton, G.D., and Vanko, D.A. (Eds.)
Proceedings of the Ocean Drilling Program, Scientific Results Volume 206

13. Data Report: Physical Properties of the Upper Oceanic Crust of ODP Site 1256: Multisensor Track and Moisture and Density Measurements[1]

Richard D. Jarrard[2] and Marcie J. Kerneklian[2,3]

ABSTRACT

Bulk density, porosity, and matrix density were measured on 88 basalt core plugs from Ocean Drilling Program Site 1256. Shipboard measurements using the multisensor track were reprocessed and edited to minimize the effects of core segmentation and calibration problems and are presented in this data report.

INTRODUCTION

This study presents new physical property measurements for the basalts from Ocean Drilling Program (ODP) Site 1256, which obtained a 502-m section of upper oceanic crust. Geophysical properties of these basalts can be determined in three ways: (1) downhole logging, (2) whole-core measurements, or (3) laboratory measurements on core plugs. All three were undertaken on board the ship during ODP Leg 206. Downhole measurements were reported by the Shipboard Scientific Party (2003b). Whole-core sections were measured on the multisensor track (MST). MST measurements, consisting of gamma ray attenuation bulk density, natural gamma ray activity, and magnetic susceptibility, were presented in the Leg 206 *Initial Reports* volume (Shipboard Scientific Party, 2003b), but they were not interpreted because of excessive noise from the broken core segments. Moisture and density (MAD) properties of 167 discrete samples were measured shipboard us-

[1]Jarrard, R.D., and Kerneklian, M.J., 2007. Data report: physical properties of the upper oceanic crust of ODP Site 1256: multisensor track and moisture and density measurements. *In* Teagle, D.A.H., Wilson, D.S., Acton, G.D., and Vanko, D.A. (Eds.), *Proc. ODP, Sci. Results,* 206: College Station, TX (Ocean Drilling Program), 1–11. doi:10.2973/odp.proc.sr.206.011.2007
[2]Department of Geology and Geophysics, University of Utah, Salt Lake City UT 84112, USA. Correspondence author: **jarrard@earth.utah.edu**
[3]Present address: Newmont Mining Corporation, Golconda NV 89414, USA.

Initial receipt: 5 July 2005
Acceptance: 20 September 2006
Web publication: 2 February 2007
Ms 206SR-011

ing a pycnometer (Shipboard Scientific Party, 2003a) and interpreted by Shipboard Scientific Party (2003b).

This study provides two complementary data sets: laboratory measurements of bulk density, porosity, and matrix (or grain) density for 88 additional core plugs, and reprocessed shipboard MST data.

METHODS

MAD Measurements

On board the ship, 88 cylindrical samples were drilled from the working halves of the Site 1256 basement cores. Sample diameters were 2.5 cm, and volumes of most samples were ~13 cm^3. Porosity, bulk density, and matrix density of the core plugs (Table T1) were determined postcruise using a simple weight-and-volume technique, as described by Brink and Jarrard (1998) and Brink (1999), with salt correction (Hamilton, 1971). Samples were evacuated for about 3 days to remove pore water, with a final vacuum pressure of 70–80 mTorr, then dry weight was measured twice. Samples were evacuated again at 70–80 mTorr for 1 day, then flooded with seawater while still under vacuum. Next, external pressure was changed to atmospheric, permitting the high vacuum within each sample's pores to suck water into its pores. Wet volume (four replicates) and wet weight (three replicates) of each sample were then measured. Accuracy of this technique was confirmed by measuring a suite of standard samples. These standards are Ferron sandstones that had previously been measured by Amoco using a helium porosimeter and mercury immersion, as described by Sondergeld and Rai (1993).

T1. New MAD measurements for minicores from Site 1256, p. 11.

The crossplots of Figure F1 compare shipboard to shore-based MAD measurements. The two data sets have generally very similar bulk densities, but they exhibit different apparent dependencies of bulk density and matrix density on porosity. We attribute this difference to incomplete drying by the shipboard method (oven drying), which results in a subtle underestimation of both matrix density and porosity. Similar offsets have been noted in some previous basalt cores (e.g., Sites 768, 770 [Jarrard and Schaar, 1991], and 801 [Jarrard et al., 2003]). The inverse correlation between matrix density and porosity is attributable to alteration-induced lowering of matrix density in high-porosity, high-permeability samples (e.g., Christensen et al., 1980; Busch et al., 1992; Jarrard et al., 2003).

F1. Shipboard vs. shore-based measurements of MAD properties, p. 7.

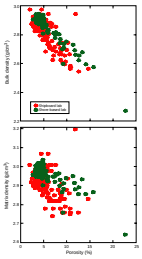

Continuous logs of bulk density as a function of depth are available from both whole-core MST measurements and well-logging (Shipboard Scientific Party, 2003b). These density logs can be converted to porosity by assuming a constant matrix density. The mean matrix density for these basalts is 2.92 g/cm^3 based on shipboard MAD measurements and 2.96 g/cm^3 based on shore-based MAD measurements.

Multisensor Track Measurements

All basalt whole cores from Site 1256 were measured on the MST. Measurement spacing was 2.5 cm for density and magnetic susceptibility and 5 cm (with a 20 s count time) for natural gamma measurements. Figure F2 shows these raw data. All three records exhibit spuriously high dispersion, resulting from the discontinuous nature of the hard rock core (empty space, plastic spacers, and rubble zones). Values for all

F2. Shipboard results of Hole 1256D MST measurements, p. 8.

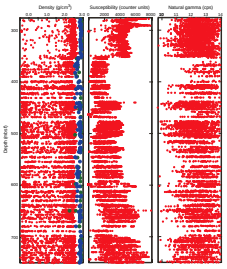

three measurements are also biased to lower values because the core diameter is less than that of the core liner. Because of these problems, which are characteristic of all ODP basalt MST measurements, some ODP legs do not undertake MST logging of basalts. Our approach, in contrast, was to take more closely spaced MST measurements than are typical, so that the effects of discontinuous core can be successfully removed postcruise.

The first step in our MST editing was to remove some depth overlaps of adjacent cores, associated with cores that had an apparent recovery of >100%. This excessive recovery results from loss of one or more core segments from the base of the overlying core, so core depths were slightly revised upward accordingly.

Our initial processing of the MST density data includes two recalibration steps. Raw gamma counts had been converted to bulk density during Leg 206, based on a regression fit of counts to density for a set of five standards. This conversion was satisfactory for Hole 1256D, but the Hole 1256C calibration led to systematic underestimation of densities by ~0.1 g/cm^3. The origin of this calibration problem is unknown, but it can be avoided by using the Hole 1256D calibration for both holes. Second, the density calculation assumes that the core liner is entirely filled with rock. This assumption is appropriate for most sediment cores, but basalt cores are mostly 58.5 mm in diameter or less, much narrower than the 66-mm internal diameter of the plastic core liner. Furthermore, this reduced diameter causes the gamma ray beam to penetrate the core 3.5 mm above its center, further reducing the effective "diameter" of core seen to 58 mm. These biases can be removed by multiplying all densities by 66/58 = 1.138.

This recalibrated density log is not yet a reliable indicator of in situ bulk densities, but it does indicate the mass of basalt seen by the magnetic susceptibility and natural gamma MST tools. Thus, we can minimize the effects of variations in core segment volume on magnetic susceptibility and natural gamma by converting these records to a mass basis.

Raw magnetic susceptibility data are in instrument units, but they can be converted to SI volume susceptibilities by multiplying by 10^{-5} times the volume correction factor of ~0.7 (Blum, 1997). We corrected for variations in core volume as follows. First, the susceptibility loop has a response function with an approximately 5-cm half-width, so we estimated this response function by noting the shape of the magnetic susceptibility responses at numerous examples of single-point density spikes: 0.05, 0.2, 0.5, 0.2, 0.05 for the five magnetic susceptibility measurements centered at the density spike. We therefore smoothed the edited MST density log with this 5-point operator. We then converted the volume susceptibility measurements to mass susceptibilities by dividing each susceptibility value by its MST density. Finally, we smoothed the resulting record with a weighted 7-point average; the weighting was 0 for raw density <0.5 g/cm^3, 1 for raw density = 0.5–2.0 g/cm^3, and 2 for raw density = >2 g/cm^3, and only depths with a total weight of at least 2 were retained.

The natural gamma instrument used on the ship records counts per second (cps), which depends on the rock volume seen by the detector crystal, the device setup, and background counts (Blum et al., 1997; Blum, 1997). A zero background spectrum is removed from each measurement, based on measurement of a liner containing water. A typical shipboard background is 8–9 cps according to Blum (1997), but the background during Leg 206 was slightly higher: the minimum raw

value was 9.75 cps. On board Leg 206, however, all data were corrected using a background of 13.99, which is too high: most corrected counts are zero. The appropriate background correction for Leg 206 is not reliably known, but it is probably ~10 cps, slightly higher than the minimum reading because of statistical fluctuations in radioactivity measurements. We therefore removed a background count of 10 cps from all measurements. If the actual background is somewhat higher or lower, the character of the final log (Figs. F3, F4) is minimally affected but the entire log is biased by a few percent.

The next step in reprocessing of the natural gamma was to delete the last four points of each section, which exhibit huge but unpredictable biases. We do not know the origin of these clearly core-edge effects; they are not tray contamination because they affect the last 3–4 points of each section regardless of its length. The natural gamma detector crystal is 7.6 cm in diameter with a spatial resolution of ~12 cm, so we smoothed the density record with a natural gamma response function consisting of a 10-cm-wide plateau and tapered flanks. We then calculated natural gamma counts per gram by dividing the natural gamma record by both measured volume and smoothed density. We applied a 7-point weighted average to the resulting record, with weighting based on density (as above) and with a minimum weight of 4 (at least two good density points) for retention of data from any depth.

Much of the MST density record exhibits density dropouts due to gaps between core pieces and the edges of core pieces. These dropouts should be retained when correcting magnetic susceptibility and natural gamma from a volume basis to weight basis, as described above. They should be deleted, however, when attempting to estimate true basalt densities. These dropouts were minimized by deleting all values <2.48 g/cm^3, based on the observation that the lowest of our 147 MAD density measurements was 2.482 g/cm^3. Note, however, that this procedure also removes potentially reliable but low density measurements for rare hyaloclastites and breccias, not sampled by MAD. We also deleted core segment-edge measurements, based on the criterion that such measurements are flanked by an adjacent blank reading and one at least 0.1 g/cm^3 higher than it. A second core segment-edge exclusion criterion was to delete dropouts of >0.15 g/cm^3 compared to its adjacent reading. These MST densities then were smoothed with a 5-point median, except across data gaps.

Finally, all three MST logs were resampled at 0.25 m spacing.

Figures F3 and F4 show the reprocessed density, magnetic susceptibility, and natural gamma records for Holes 1256C and 1256D. Also shown in these figures are the MAD measurements (new and shipboard) of bulk density. These minicore measurements are generally consistent with the reprocessed densities, whereas they were much higher than the raw MST densities shown in the Leg 206 *Initial Reports* volume and in Figure F1. Hole 1256D was logged with the lithodensity well-logging tool, but this log exhibits too many washout-induced artifacts for direct comparison. Both density and resistivity depend mainly on porosity, but resistivity logs are much less sensitive to washouts. We therefore overlay a 10-m averaged resistivity log on the MST densities of Figure F4, confirming that the broad patterns of the two are consistent. Unlike the resistivity log, however, MST densities fail to sample macroporosity such as large fractures and interflow voids (e.g., Jarrard et al., 2003).

The reprocessed natural gamma record exhibits abundant spikes to high gamma counts. These are unlikely to be artifacts due to underesti-

F3. Reprocessed MST measurements of the basalts of Hole 1256C, p. 9.

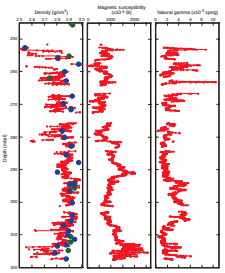

F4. Reprocessed MST measurements of the basalts of Hole 1256D, p. 10.

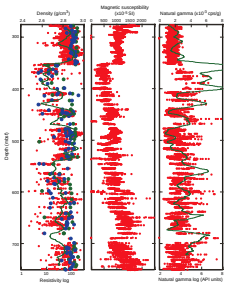

mation of density, because the magnetic susceptibility record lacks analogous spikes. More likely, they result from local potassium enrichment due to basalt alteration or magmatic fractionation. The downhole spectral gamma log (Shipboard Scientific Party, 2003b) also shows abundant spikes to high natural gamma counts, though it averages a much longer depth interval. Figure **F4,** which overlays a 10-m averaged downhole natural gamma log on the edited MST log for Hole 1256D, shows the impact of alteration on core recovery. In intervals with high core recovery and therefore densely sampled MST readings (e.g., above 350 meters below seafloor [mbsf] and at ~410, 450, and 480 mbsf), both MST and logging natural gamma counts exhibit minimum values. In intervals with very high natural gamma counts on the well log, core recovery and MST data are sparse. The downhole log indicates that total natural gamma counts are primarily associated with potassium variations, with consistently very low contributions to total counts from uranium and thorium.

ACKNOWLEDGMENTS

We thank the scientific party of ODP Leg 206 for shipboard advice and collaboration. This research used samples and data provided by the Ocean Drilling Program (ODP). ODP is sponsored by the U.S. National Science Foundation (NSF) and participating countries under management of Joint Oceanographic Institutions (JOI), Inc. Funding for this research was provided to M.J. Kerneklian and R.D. Jarrard by the U.S. Science Support Program.

REFERENCES

Blum, P., 1997. Physical properties handbook: a guide to the shipboard measurement of physical properties of deep-sea cores. *ODP Tech. Note,* 26 [Online]. Available from World Wide Web: <**http://www-odp.tamu.edu/publications/tnotes/tn26/INDEX.HTM**>. [Cited 2001-09-02]

Blum, P., Rabaute, A., Gaudon, P., and Allan, J.F., 1997. Analysis of natural gamma-ray spectra obtained from sediment cores with the shipboard scintillation detector of the Ocean Drilling Program: example from Leg 156. *In* Shipley, T.H., Ogawa, Y., Blum, P., and Bahr, J.M. (Eds.), *Proc. ODP, Sci. Results,* 156: College Station, TX (Ocean Drilling Program), 183–195. **doi:10.2973/odp.proc.sr.156.024.1997**

Brink, J.D., 1999. Petrophysics and log-based sedimentology of the Cape Roberts project, Antarctica [M.S. thesis]. Univ. of Utah, Salt Lake City.

Brink, J.D., and Jarrard, R.D., 1998. Petrophysics of core plugs from CRP-1 drillhole, Victoria land basin, Antarctica. *In* Barrett, P.J., and Ricci, C.A. (Eds.), *Studies from the Cape Roberts Project, Ross Sea, Antarctica—Scientific Report of CRP-1*. Terra Antart., 5(3):291–298.

Busch, W.H., Castillo, P.R., Floyd, P.A., and Cameron, G., 1992. Effects of alteration of physical properties of basalts from the Pigafetta and East Mariana basins. *In* Larson, R.L., Lancelot, Y., et al., *Proc. ODP, Sci. Results,* 129: College Station, TX (Ocean Drilling Program), 485–499. **doi:10.2973/odp.proc.sr.129.139.1992**

Christensen, N.I., Blair, S.C., Wilkens, R.H., and Salisbury, M.H., 1980. Compressional wave velocities, densities, and porosities of basalts from Holes 417A, 417D, and 418A, Deep Sea Drilling Project Legs 51–53. *In* Donnelly, T., Francheteau, J., Bryan, W., Robinson, P., Flower, M., Salisbury, M., et al., *Init. Repts. DSDP,* 51, 52, 53 (Pt. 2): Washington (U.S. Govt. Printing Office), 1467–1471.

Hamilton, E.L., 1971. Prediction of in-situ acoustic and elastic properties of marine sediments. *Geophysics,* 36:266–284.

Jarrard, R.D., Abrams, L.J., Pockalny, R., Larson, R.L., and Hirono, T., 2003. Physical properties of upper oceanic crust: Ocean Drilling Program Hole 801C and the waning of hydrothermal circulation. *J. Geophys. Res.,* 108(B4):2188. **doi:10.1029/2001JB001727**

Jarrard, R.D., and Schaar, R., 1991. Electrical properties of basalts from Site 768 and 770. *In* Silver, E.A., Rangin, C., von Breymann, M.T., et al., *Proc. ODP, Sci. Results,* 124: College Station, TX (Ocean Drilling Program), 91–104. **doi:10.2973/odp.proc.sr.124.172.1991**

Shipboard Scientific Party, 2003a. Explanatory notes. *In* Wilson, D.S., Teagle, D.A.H., Acton, G.D., *Proc. ODP, Init. Repts.,* 206: College Station, TX (Ocean Drilling Program), 1–94. **doi:10.2973/odp.proc.ir.206.102.2003**

Shipboard Scientific Party, 2003b. Site 1256. *In* Wilson, D.S., Teagle, D.A.H., Acton, G.D., *Proc. ODP, Init. Repts.,* 206: College Station, TX (Ocean Drilling Program), 1–396. **doi:10.2973/odp.proc.ir.206.103.2003**

Sondergeld, C.H., and Rai, C.S., 1993. A new exploration tool: quantitative core characterization. *Pure Appl. Geophys.,* 141(2–4):249–268. **doi:10.1007/BF00998331**

Figure F1. Comparison of shipboard and shore-based (this study) measurements of MAD properties for the basalts of Site 1256. The slightly lower trends for shipboard measurements (red dots) are attributed to incomplete drying.

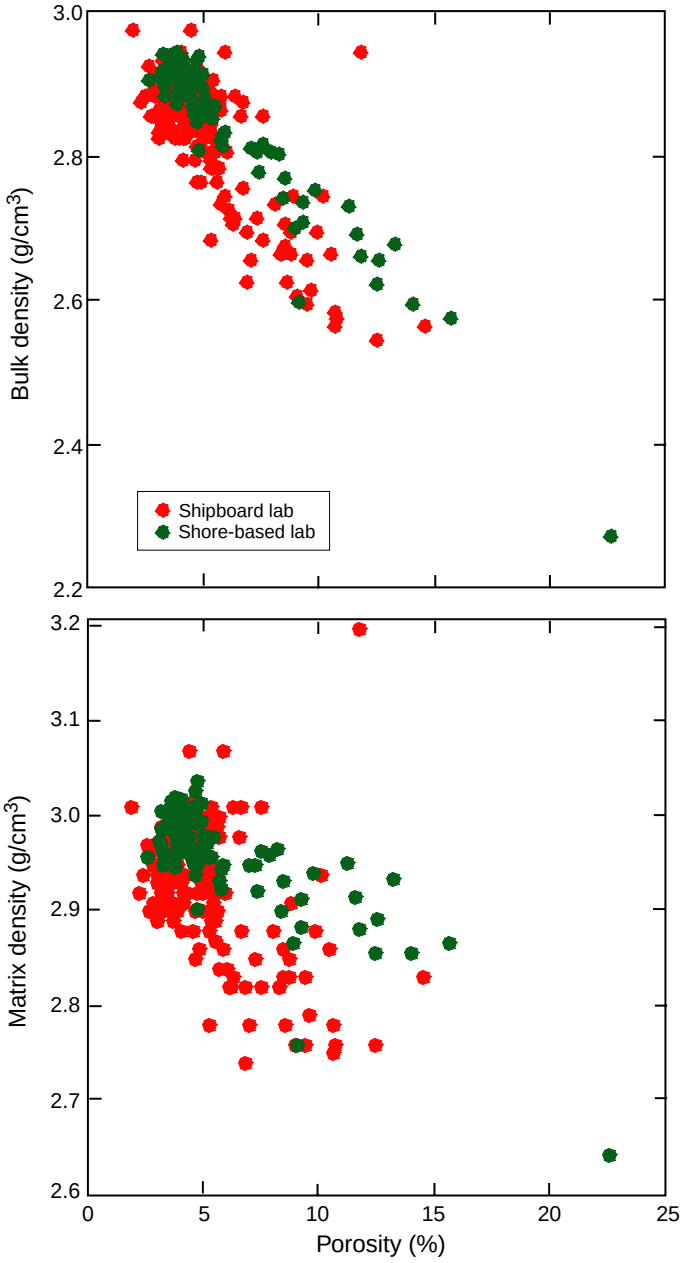

Figure F2. Shipboard results of multisensor track (MST) measurements of the basalts of Hole 1256D. Note the consistently much lower bulk densities recorded by the MST (red dots) than by shipboard (blue dots) and shore-based (green dots) index measurements on discrete samples. cps = counts per second.

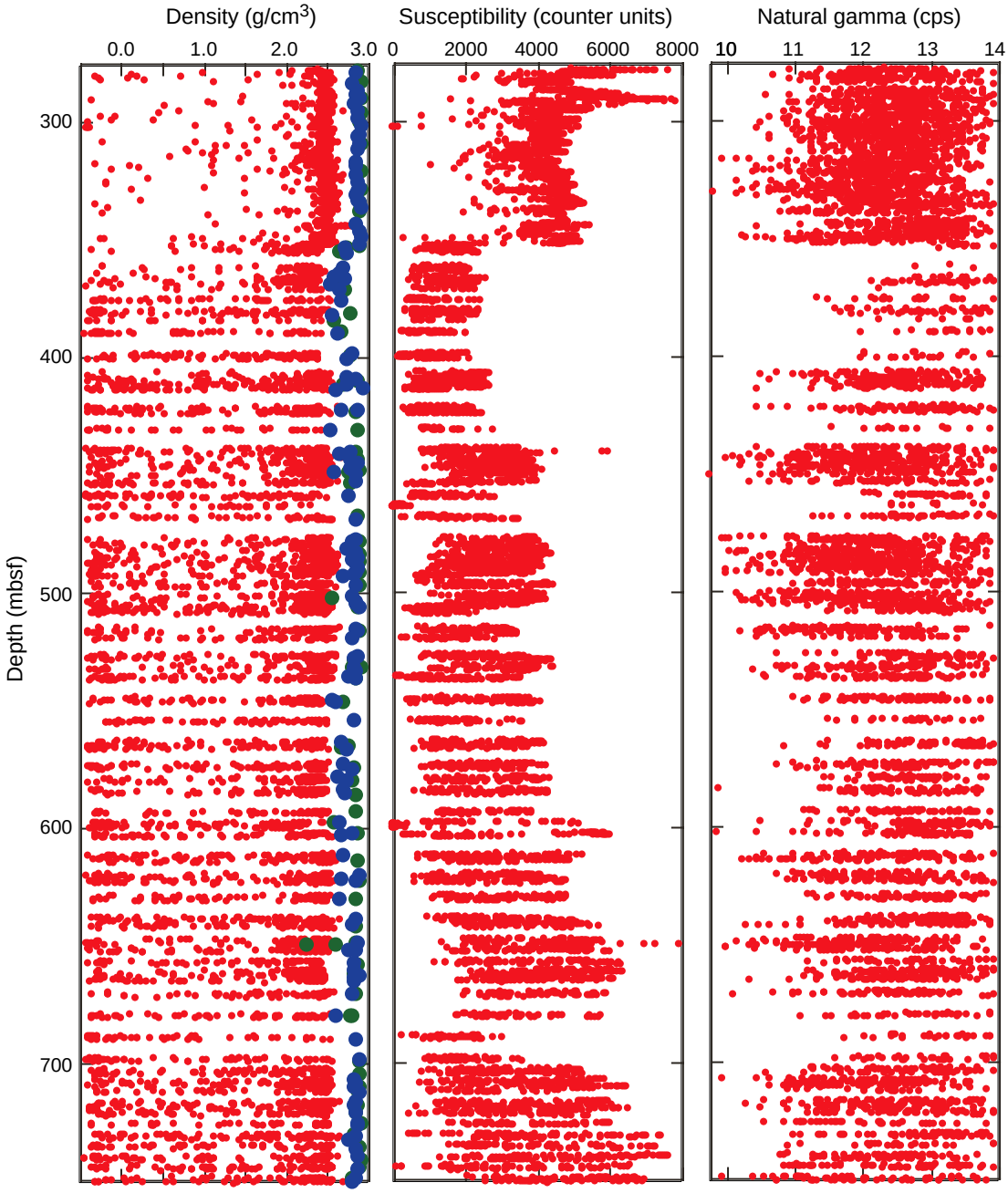

Figure F3. Multisensor track (MST) measurements of the basalts of Hole 1256C after the reprocessing of this study. Note the general agreement of MST data (red dots) with shipboard (blue dots) and shore-based (green dots) index measurements on discrete samples. cps = counts per second.

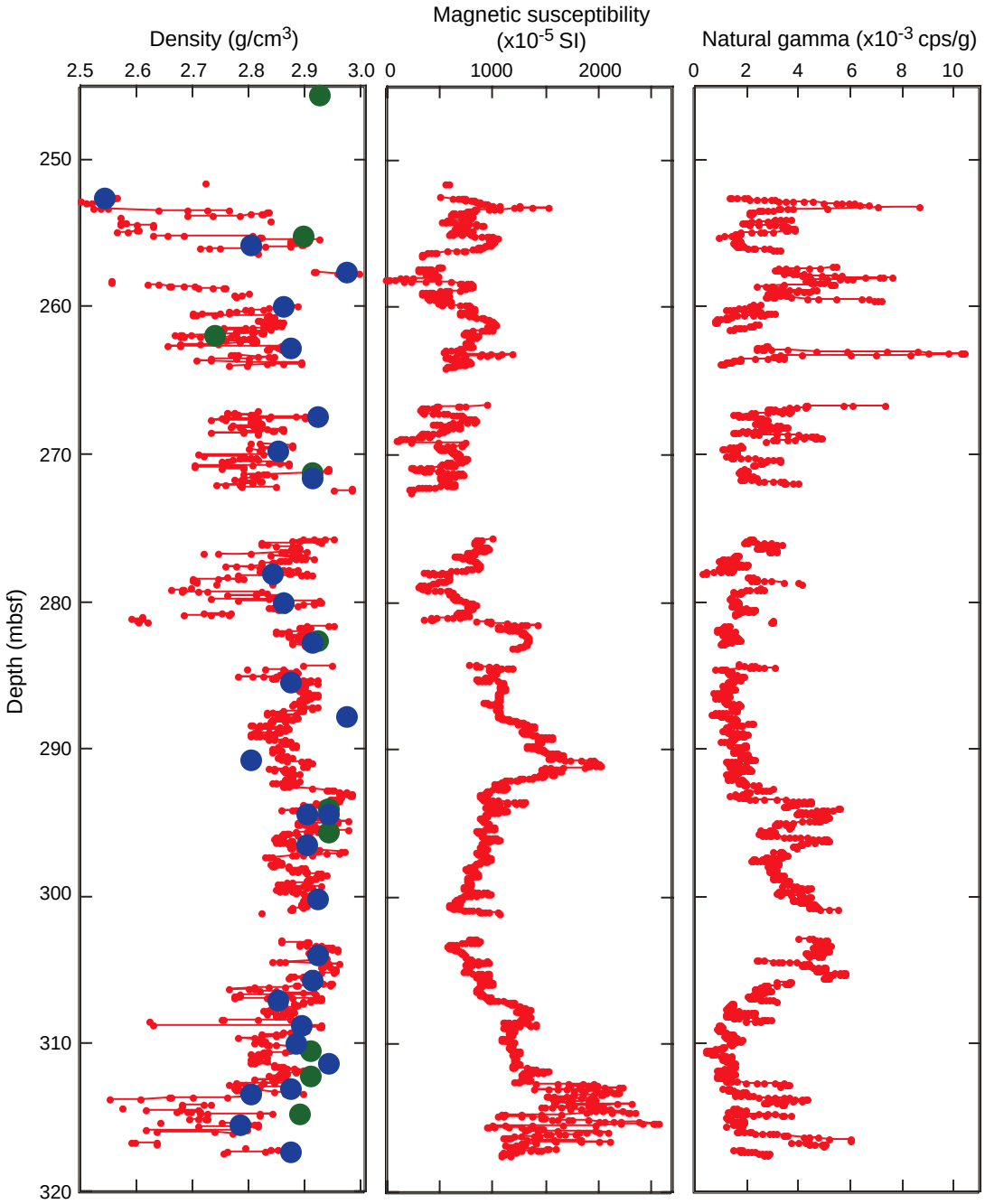

Figure F4. Multisensor track (MST) measurements of the basalts of Hole 1256D after the reprocessing of this study. Note the general agreement of MST data (red dots) with shipboard (blue dots) and shore-based (green dots) index measurements on discrete samples. Resistivity and natural gamma well logs (green lines) are overlain on the MST data to show the broad patterns of expected MST variations. cps = counts per second. API = American Petroleum Institute units.

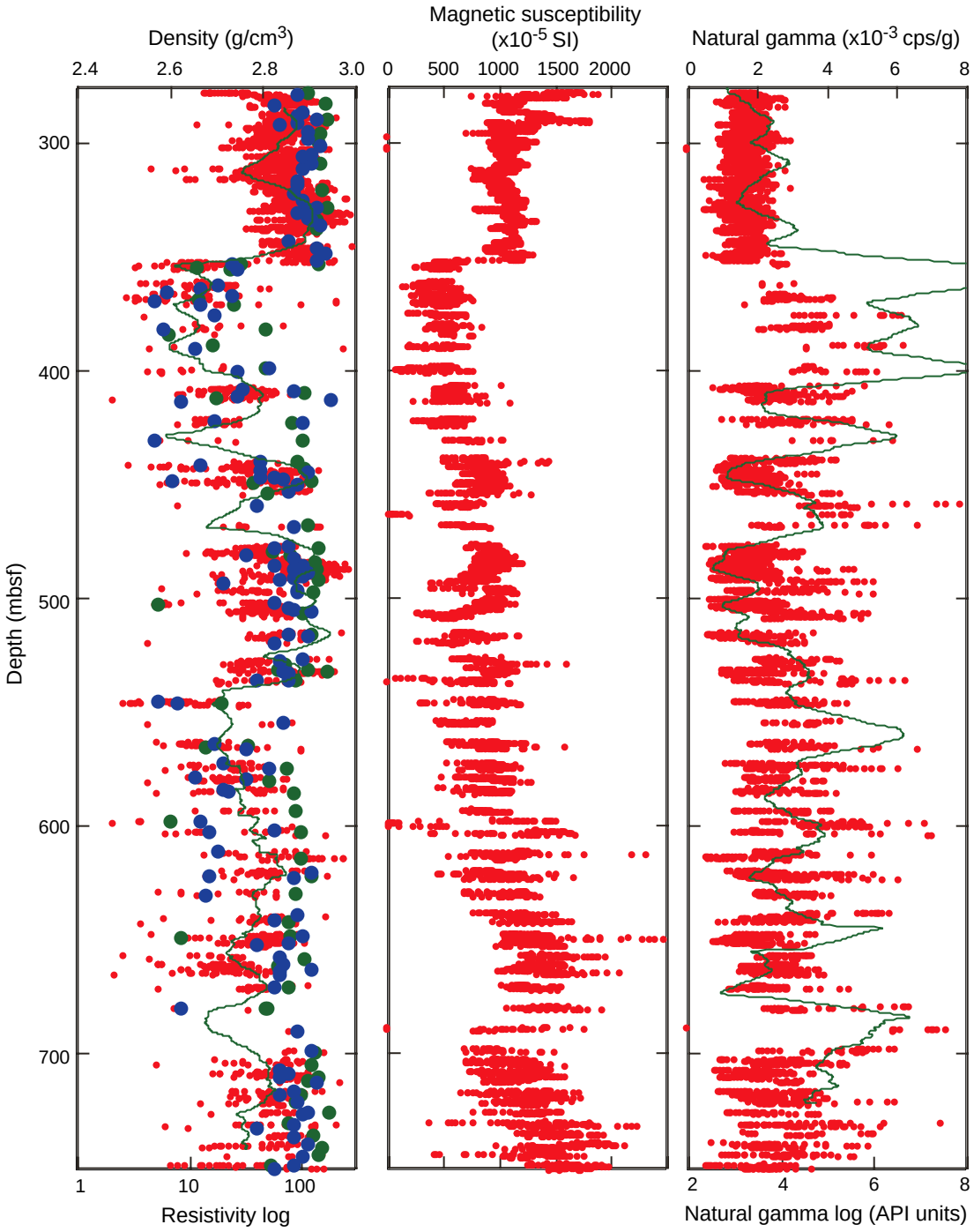

Table T1. New MAD measurements for minicores from Site 1256.

Core, section, interval (cm)	Depth (mbsf)	Bulk density (g/cm^3)	Porosity (%)	Matrix density (g/cm^3)
206-1256C-				
4R-1, 49–51	245.49	2.93	3.8	3.01
5R-2, 121–133	255.10	2.90	4.6	2.99
6R-4, 74–76	261.81	2.75	8.2	2.90
7R-5, 17–19	271.08	2.92	3.6	2.99
8R-6, 107–109	282.53	2.93	3.3	2.99
9R-7, 77–79	293.85	2.95	3.7	3.02
10R-2, 10–12	295.45	2.95	3.5	3.02
11R-5, 105–107	310.27	2.92	4.2	3.00
11R-7, 5–7	312.09	2.92	4.5	3.01
12R-2, 36–38	314.60	2.90	4.3	2.98
206-1256D-				
2R-1, 14–16	276.24	2.90	4.8	3.00
3R-3, 92–74	281.44	2.94	4.5	3.03
4R-3, 47–49	288.17	2.94	4.6	3.04
5R-4, 49–51	294.29	2.93	3.8	3.01
6R-3, 81–83	298.02	2.92	3.7	3.00
7R-3, 110–112	307.78	2.93	4.0	3.01
8R-6, 30–32	319.41	2.93	3.8	3.01
9R-4, 89–91	327.26	2.94	3.9	3.02
10R-4, 112–114	332.15	2.92	4.8	3.02
11R-4, 48–50	336.12	2.92	3.9	3.00
12R-8, 83–85	351.33	2.93	3.1	2.99
13R-1, 141–143	351.71	2.76	9.6	2.94
13R-3, 38–40	353.62	2.66	12.4	2.89
13R-3, 66–68	353.90	2.74	11.1	2.95
15R-2, 113–115	366.83	2.67	11.6	2.88
16R-1, 96–98	369.86	2.74	9.1	2.91
18R-2, 81–83	380.07	2.81	7.8	2.96
19R-1, 7–9	382.77	2.60	13.9	2.86
20R-1, 21–23	387.61	2.70	11.5	2.92
21R-1, 64–66	397.44	2.81	8.1	2.97
22R-3, 6–8	408.61	2.89	4.0	2.97
23R-1, 13–15	410.43	2.71	8.8	2.87
24R-2, 87–89	421.83	2.87	4.5	2.96
25R-1, 78–80	429.58	2.89	3.8	2.96
26R-1, 50–52	438.80	2.88	3.7	2.95
26R-3, 75–77	441.67	2.89	3.7	2.97
27R-1, 127–129	446.67	2.91	3.6	2.98
27R-2, 73–75	447.57	2.78	7.2	2.92
28R-1, 128–130	452.18	2.81	4.6	2.90
31R-1, 21–23	466.21	2.90	4.1	2.98
32R-1, 129–131	476.49	2.93	3.1	2.99
32R-2, 140–142	478.05	2.83	5.5	2.93
32R-4, 14–16	479.46	2.86	4.5	2.95
32R-2, 28–30	482.58	2.92	3.8	2.99
34R-1, 106–108	485.46	2.92	3.6	2.99
35R-2, 11–13	490.36	2.92	3.4	2.99
36R-2, 12–14	495.57	2.91	3.6	2.98
37R-1, 80–82	500.90	2.58	15.5	2.87
38R-1, 51–53	504.81	2.89	3.1	2.95
39R-1, 118–120	514.68	2.91	3.1	2.97
41R-2, 132–134	527.32	2.85	4.5	2.94
42R-1, 70–72	530.10	2.90	3.1	2.96
42R-1, 89–91	530.29	2.84	5.6	2.95
42R-1, 102–104	530.42	2.94	3.4	3.01
43R-1, 91–93	534.81	2.87	5.1	2.97
44R-2, 36–38	544.96	2.71	9.1	2.88
46R-2, 109–111	563.60	2.77	8.3	2.93
46R-3, 37–39	564.32	2.68	13.1	2.93
47R-2, 90–92	573.40	2.86	5.2	2.96
48R-2, 17–19	578.45	2.82	5.6	2.93
49R-2, 136–138	584.47	2.87	4.8	2.97
50R-1, 32–34	591.82	2.88	4.8	2.97
51R-1, 54–56	596.64	2.60	9.0	2.76
52R-1, 24–26	600.94	2.89	4.9	2.98
53R-3, 18–20	612.92	2.89	4.3	2.97
54R-2, 136–138	620.89	2.91	3.6	2.98
55R-1, 132–134	628.72	2.88	5.3	2.98
56R-3, 109–111	640.65	2.86	5.1	2.96
57R-2, 44–46	647.29	2.87	4.9	2.96
57R-2, 112–114	647.97	2.63	12.4	2.86
57R-3, 10–12	648.35	2.28	22.5	2.64
58R-2, 41–43	656.71	2.90	3.8	2.97
59R-2, 3–5	660.40	2.84	5.7	2.95
60R-1, 85–87	669.45	2.86	4.6	2.95
61R-1, 39–41	678.39	2.81	7.1	2.95
61R-1, 77–79	678.77	2.82	6.9	2.95
63R-1, 140–142	697.90	2.92	3.0	2.98
64R-2, 90–92	703.45	2.91	2.4	2.96
65R-3, 62–64	709.14	2.92	4.4	3.01
66R-1, 9–11	710.49	2.90	3.9	2.98
67R-2, 14–16	716.38	2.89	3.6	2.96
68R-1, 48–50	719.98	2.87	4.3	2.96
69R-1, 65–67	724.75	2.95	3.0	3.01
70R-1, 26–28	728.96	2.86	5.1	2.96
71R-1, 125–127	734.55	2.91	4.0	2.99
72R-2, 32–34	739.72	2.93	3.5	3.00
73R-1, 56–58	742.96	2.92	4.4	3.01
74R-1, 49–51	747.69	2.82	7.4	2.96